ACS Energy LETTERS

http://pubs.acs.org/journal/aelccp

LETTER

Light and Thermally Induced Evolutional Charge Transport in $CH_3NH_3PbI_3$ Perovskite Solar Cells

Jiajun Peng,[†] Yong Sun,[†] Yani Chen,[†] Yao Yao,*[,‡] and Ziqi Liang*[,†]

[†]Department of Materials Science, Fudan University, Shanghai 200433, China

[‡]State Key Laboratory of Surface Physics and Department of Physics, Fudan University, Shanghai 200433, China

Supporting Information

ABSTRACT: **Pre-exposure of perovskite solar cells to light or heat can greatly improve their performance, yet the underlying physical mechanisms are still obscure. Herein we systematically investigate the influences of light soaking and thermal phase transition on charge transport dynamics in two-step fabricated $CH_3NH_3PbI_3$ perovskite solar cells. By applying the time-of-flight (TOF) measurement under various light illumination times, we not only confirm the existence of nondispersive charge transport in perovskite solar cells but also directly observe a shallow trap filling process and thus increased charge mobility upon light soaking. We further employ the delay-time-dependent charge extraction by linearly increasing voltage (CELIV) technique to reveal that dispersive bimolecular recombination is also largely inhibited. On the other hand, we conduct temperature-dependent TOF and electrical conductivity studies and surprisingly find a rapid change of both hole and electron mobilities during phase transition from tetragonal to cubic crystalline structures at around 310−330 K until reaching a balance of charge transport.**

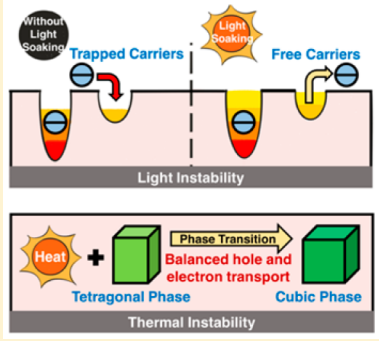

Thin-film solar cells have recently encountered an unprecedented opportunity with the appearance of almighty organic−inorganic hybrid perovskites ($CH_3NH_3PbX_3$, X = I, Br, Cl), which exhibit a broad optical absorption range,[1] low exciton binding energy,[2] long charge diffusion length,[3] and high charge mobility.[4] With enormous efforts of morphology optimization, the certified power conversion efficiency (PCE) of perovskite solar cells has skyrocketed to 22.1% in 2016 from 3.8% in 2009, which remarkably overwhelms conventional thin-film organic cells.[5,6]

However, perovskite solar cells are highly sensitive to the operational environment such as moisture, light, and heat, which stands out among the biggest hurdles toward future large-scale application of perovskite solar cells.[7−15] Despite a well-known moisture instability issue, it was recently unveiled that prelight or -heat exposure can greatly improve the performance of working perovskite solar cells; however, the underlying physical mechanisms, especially the charge transport dynamics, are still very obscure.[10,11] For instance, it was found that a light-induced self-poling effect[9] and annihilation of Frenkel defects[15] commonly existed in perovskite solar cells, and the light soaking process could noticeably enhance the PCE by decreasing interfacial charge accumulation, bulk defects, and polarizations.[10] Yet, how light illumination impacts the charge transport process of perovskite solar cells remains unclear. Meanwhile, the device performance was found to be highly sensitive to the working temperature.[11−14] For example, Leong et al. reported that the PCE of perovskite solar cells had a positive temperature coefficient for $T < 330$ K and the best value at 330 K,[11] which is consistent with previous reports that phase transition can easily switch from tetragonal to cubic crystalline at around 310−330 K.[12−14]

We have recently demonstrated that charge extraction by linearly increasing voltage (CELIV) and time-of-flight (TOF) can be utilized as effective tools to reveal efficient and balanced charge transport in one-step fabricated perovskite solar cells.[16] CELIV can measure charge mobility and investigate the recombination process in working solar cells; however, it cannot distinguish the type of charge carriers—hole or electron.[17] By contrast, TOF can measure both hole and electron mobilities and determine different levels of trap states, while a relatively thick film is required to ensure that charge carriers traverse the depletion region to reach accurate values of the TOF mobility.[18]

In this work, we extend both CELIV and TOF measurements to two-step fabricated $CH_3NH_3PbI_3$ perovskite solar cells, which exhibit higher PCEs yet often require pre-exposure of light and heat to achieve the best performance.[10,11,19] By applying illumination and temperature-dependent TOF and

Received: August 29, 2016
Accepted: October 18, 2016
Published: October 18, 2016

DOI: 10.1021/acsenergylett.6b00393
ACS Energy Lett. 2016, 1, 1000−1006

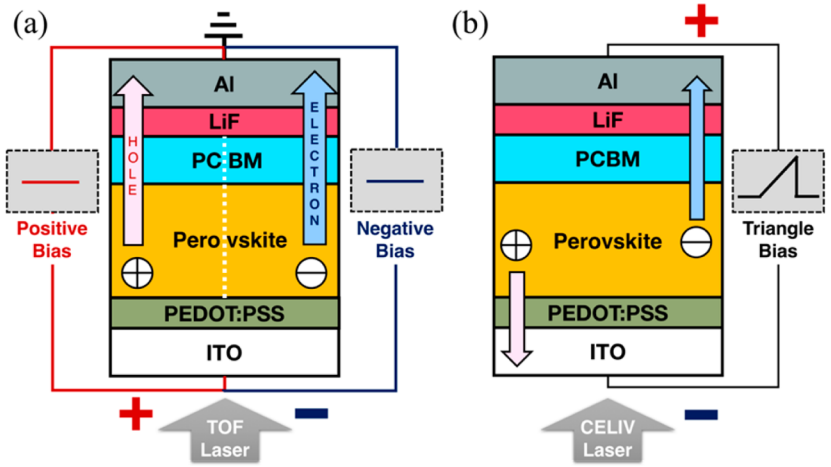

Figure 1. Schematic of (a) TOF and (b) CELIV measurements on the two-step fabricated perovskite solar cells.

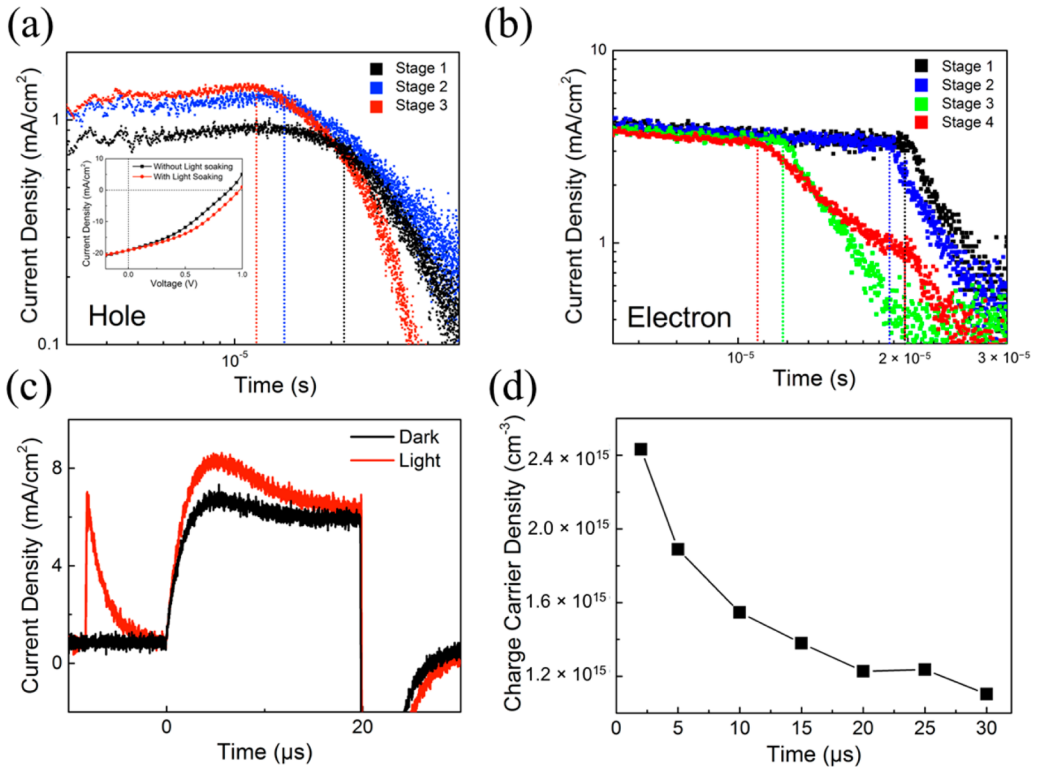

Figure 2. Temporal dependent transport dynamics of $CH_3NH_3PbI_3/PC_{61}BM$ bilayer cells upon light illumination. (a) TOF hole and (b) electron $j-t$ profiles at an applied bias of 2 V with prolonged light illumination. The inset image shows the $J-V$ curves measured without and with the light soaking step. Note that stages 1−3 in the hole measurement represent $j-t$ curves acquired by averaging 32, 64, and 128 frames, respectively, while stages 1−4 in the electron measurement correspond to averaging 8, 16, 32, and 64 frames, respectively. The vertical dotted line indicates t_{tr}. (c) Dark- and photo-CELIV $j-t$ profiles of $CH_3NH_3PbI_3/PC_{61}BM$ bilayer cells at a voltage ramp of 1×10^5 V/s and at a delay time of 8 μs and (d) their photogenerated carrier density versus delay time curve.

CELIV, we seek to investigate the influences of light soaking and phase transition on transport dynamics, respectively. Upon continuous light illumination, we directly observe a shallow trap filling process, indicating that light soaking can strongly reduce trap-assisted charge recombination and thus remarkably increase both hole and electron mobilities in perovskite solar cells. Meanwhile, we find that dispersive bimolecular charge recombination is also largely suppressed. On the other hand, during phase transition from 310 to 330 K, hole mobility is found to decrease while electron mobility increases until both of them reach a balance, which is supported by the unchanged electrical conductivity and is also in good agreement with the best cell performance obtained in a previous report.[11]

Typical perovskite-based solar cells were fabricated on the device configuration of ITO/PEDOT:PSS (50 nm)/two-step $CH_3NH_3PbI_3$ (350 nm)/phenyl-C61-butyric acid methyl ester (PCBM, 100 nm)/LiF (1 nm)/Al (100 nm) with an active area of 0.11 cm^2, as illustrated in Figure S1a. Their representative photocurrent densities versus voltage ($J-V$) curves under simulated AM 1.5G at both forward and reverse scans of sunlight are displayed in Figure S1b. At forward scan, the device exhibits a PCE of 12.3% with a short-circuit current density

DOI: 10.1021/acsenergylett.6b00393
ACS Energy Lett. 2016, 1, 1000−1006

(J_{SC}) of 18.88 mA/cm^2, an open-circuit voltage (V_{OC}) of 1.05 V, and a fill factor (FF) of 62%. By contrast, a higher PCE of 14.4% is obtained at reverse scan, primarily resulting from a higher FF of 73% while preserving a J_{SC} of 18.71 mA/cm^2 and V_{OC} of 1.05 V.

We then utilized both TOF and CELIV measurements to systematically investigate transport dynamics in the above two-step fabricated perovskite solar cells. Both methods are schematically shown in Figure 1. In the TOF measurement, fixed positive and negative biases were applied to measure the hole and electron mobilities, respectively (Figure 1a).[18] Both photogenerated hole and electron carriers in the TOF measurement will transport from the perovskite layer to the PCBM layer, followed by charge collection at the Al electrode. The TOF mobilities are calculated from eq 1[18]

$$\mu = \frac{d^2}{V \cdot t_{tr}} \tag{1}$$

where μ is the charge mobility, d is the thickness of the active layer, V is the voltage bias, and t_{tr} is the transient time. Here, we aim to apply the TOF technique to study the influences of light soaking and phase transition on the charge transport process of perovskite solar cells. By contrast, in CELIV measurements, a triangle voltage is applied to measure the charge mobility and study the recombination process (Figure 1b).[18] Photogenerated holes will only traverse the perovskite layer only and then get collected at the ITO electrode, while electrons will transport from the perovskite to PCBM and then get collected at the Al electrode. The CELIV mobility is calculated from eq 2[18]

$$\mu = \frac{2d^2}{3\frac{\Delta U}{\Delta t} \cdot t_{max}^{\ 2}} \tag{2}$$

where μ is the carrier mobility, d is the thickness of the active layer, $\Delta U/\Delta t$ is the voltage ramp of the applied triangle voltage pulse, and t_{max} is the time when the value of the current density is maximum. However, because of the ambipolar nature of perovskite, it is difficult to distinguish between hole and electron carriers by the CELIV technique.[18]

It is worth noting that the charge transporting layer in both TOF and CELIV measurements in the above perovskite solar cells is composed of both two-step $CH_3NH_3PbI_3$ and PCBM layers instead of a single perovskite or PCBM layer. Because of the nonexciton nature of the perovskite that typically has a small exciton binding energy of 50 meV,[2,20,21] charge dissociation occurs immediately after photogeneration, which efficiently produces free carriers within the inner perovskite layer rather than at the $CH_3NH_3PbI_3$/PCBM interface. In addition, charge mobilities of both neat perovskite and neat PCBM films as measured by CELIV and TOF were reported on the similar order of 10^{-3}–10^{-4} cm^2/(V s),[16,22,23] which further supports that both perovskite and PCBM contribute to the charge transporting layer.

We first applied TOF measurement to investigate the influences of light illumination on transport dynamics of the above perovskite solar cells. Figure 2 presents current density versus time (j–t) profiles with increasing illumination time. Such an evolutional process has not been observed yet in the one-step fabricated perovskite solar cells. Note that the increasing illumination time of the laser light in the TOF technique was made by acquiring j–t curves by increasing average frames, which is equivalent to light soaking in J–V measurements. Our experiments cover the largest spectrum of device conditions—from an initial state without light soaking, to an intermediate state during light soaking, and finally to a stable state after light soaking. Therefore, the temporal TOF study offers an excellent means of unraveling the role of light soaking in charge transport process.

Superior TOF transients with a distinct plateau are observed from Figure 2a,b for holes and, more remarkably, electrons, respectively, which provides strong evidence of nondispersive charge transport in perovskite solar cells. This is distinctive from dispersive transport of most organic semiconductors and their solar cells, which is often caused by the existence of disordered structures and deep-level traps.[18] Therefore, this result interprets well why perovskite solar cells outperform organic solar cells, owing to the large tolerance of trap states and high crystallinity in perovskites.[24,25] Note that we observe a more distinct plateau of TOF curves when measuring electron mobility in this work than the PCBM electron measurement in any other work,[22,23] indicating that the perovskite layer plays a dominant role in determining electron mobility than PCBM in TOF measurements.

As shown in Figure 2a,b, both hole and electron mobilities are gradually increased with prolonged light illumination. From the initial to final stage of TOF results, the hole mobility is increased from 4.62×10^{-5} to 8.65×10^{-5} cm^2/(V s), while the electron mobility is increased from 5.14×10^{-5} to 9.38×10^{-5} cm^2/(V s). Such an evolutional effect is first reversible upon initial light exposure and then reaches stable equilibrium after several minutes, which is consistent with the light soaking time scale in J–V measurement to increase the PCE and also presumably indicates the absence of ionic motion.[11] Therefore, our work demonstrates that the light soaking process can significantly improve charge transport and hence device performance.

More importantly, there is only one plateau region in the j–t curves of hole measurement, whereas there are two in those of the electron measurement. According to previous studies by the Qiu group,[26] the position of the plateau region represents the extraction of photogenerated charge carriers previously filled in the same level of trap states. The former plateau region with a shorter t_{tr} represents higher charge mobility caused by deep traps, while the latter with a longer t_{tr} suggests lower charge mobility affected by shallow traps.

Hole transport is found to be influenced only by deep traps, and hole mobility is gradually increased with an increase of illumination time. By contrast, additional shallow traps exist along the path of electron transport. This is supposed to stem from the defects at the interfaces of $CH_3NH_3PbI_3$/PCBM, which largely decrease the electron mobility. As illustrated in Figure 2a,b, with longer illumination time, the current density influenced by shallow traps is gradually decreased because more shallow traps are filled by photogenerated electrons and hence no longer hinder electron transport. Therefore, upon continuous light illumination, an evolutional process of shallow trap filling during light soaking is for the first time directly observed in TOF measurements, indicating the important role of light soaking on decreasing the charge trapping rate in perovskite solar cells.

To verify the above TOF results, the J–V curves without and with the light soaking process are both measured in the working perovskite solar cells. As shown in the inset image of Figure 2a, after continuous light illumination, V_{OC} is remarkably increased from 0.9 to 1.0 V while J_{SC} remains almost the same at 19.11

DOI: 10.1021/acsenergylett.6b00393
ACS Energy Lett. 2016, 1, 1000–1006

Table 1. Parameters Derived from Both Dark- And Photo-CELIV Curves

μ ($cm^2/(V\ s)$)	$n(0)$ (cm^{-3})	α	τ_B (s)	γ	β_L (cm^3/s)
5.29×10^{-4}	2.98×10^{15}	−0.286	1.28×10^{-5}	0.686	2.99×10^{-11}

mA/cm^2. This can be interpreted by the relationship of V_{OC} and J_{SC} as expressed by eq 3[27]

$$qV_{oc} = AkT \ln\left(\frac{J_{SC}}{J_S} + 1\right) \tag{3}$$

where A is the ideality factor, k is the Boltzmann constant, T is the temperature and J_S is the saturation current density at reverse bias. Note that J_S is defined as the recombination current density when the applied voltage is 0 V, which is independent of light illumination. According to eq 3, if J_{SC} and J_S remain unchanged, the increase of V_{OC} comes from the increase of A. It has been previously reported that the increased A mainly resulted from decreased trap-assisted recombination.[28] Therefore, the observed phenomenon of an increase of V_{OC} accompanied by constant J_{SC} clearly indicates the existence of trap-assisted charge recombination in perovskite solar cells, which agrees well with the TOF results—light soaking aids in filling shallow traps and hence greatly improving the cell performance.

In order to support our assumption on the presence of morphological defects, field emission scanning electron microscopy (FE-SEM) images were characterized to examine the interfaces between $CH_3NH_3PbI_3$ and PCBM. As shown in Figure S2a, a rough surface consisting of numerous packed crystals is found in $CH_3NH_3PbI_3$ neat film. By contrast, after deposition of the PCBM layer, the gaps between adjacent $CH_3NH_3PbI_3$ crystals are filled by PCBM and a smooth surface is thus obtained, as shown in Figure S2b. However, the cross-sectional image of $CH_3NH_3PbI_3$/PCBM in Figure S2c shows that small defects can still be found at the interfaces between $CH_3NH_3PbI_3$ and PCBM, which presumably gives rise to shallow traps and hence hinders electron transport.

As discussed above, trap-assisted charge recombination exists in perovskite solar cells. The CELIV technique was carried out to complementarily investigate the charge recombination process in the dark and under laser light illumination, and the results are shown in Figure 2c. Given a voltage ramp of 1×10^5 V/s, an overall charge mobility of 5.29×10^{-4} $cm^2/(V\ s)$ is obtained, which is quite close to that of the one-step analogous solar cell in our previous work and the CELIV result of the Park group.[16,29] This means that the transport dynamics in both one-step and two-step fabricated perovskite solar cells are similar except for the requirement of light soaking in the two-step system, as discussed previously. Note that the CELIV mobility of working perovskite solar cells is in good agreement with the TOF mobility, and both of them are different than the mobility values of 1−10 $cm^2/(V\ s)$ obtained from contact-free measurements on perovskite films by transient absorption, photoluminescence quenching, impedance spectroscopy, time-resolved microwave conductivity, time-resolved terahertz spectroscopy, and so on.[30−35]

Next, the intrinsic carrier density, which can be derived from the dark CELIV curve shown in Figure 2c,[17] is calculated as 7.73×10^{14} cm^{-3}, which is positively correlated to the trap density. Note that the Huang group recently reported the hole trap density of 2.0×10^{15} cm^{-3} in the single-layered $CH_3NH_3PbI_3$ structure,[36] which is an order of magnitude higher than the intrinsic carrier density in the bilayer structure of $CH_3NH_3PbI_3$/PCBM in our work. This suggests that introduction of a PCBM layer can greatly suppress trap states in perovskite solar cells.

To further investigate charge photogeneration and recombination processes in $CH_3NH_3PbI_3/PC_{61}BM$ bilayer cells, photo-CELIV experiments with various delay times were conducted to obtain the profiles of charge carrier density versus delay time. Note that the delay time is defined as the time between the light pulse and charge extraction. As shown in Figure 2d, the carrier density is gradually decreased from 2.43×10^{15} to 1.10×10^{15} cm^{-3} when the delay time is increased from 2 to 30 μs. More importantly, a power law dependence is found with the delay time, that is, $n(t) \propto t^{\alpha}$, where t is the delay time, $n(t)$ is the corresponding charge carrier density, and α is the free carrier recombination rate. By fitting the curve in Figure 2d to the above formula, the initial photogenerated carrier density $n(0)$ and α can be extrapolated as 2.98×10^{15} cm^{-3} and −0.286, respectively. Note that this α value of the perovskite is much lower than that of typical organic photovoltaic materials such as the blend of poly(3-hexylthiophene) (P3HT) and PCBM ($\alpha = -0.8$).[37] This also indicates that the recombination process is largely suppressed in perovskite solar cells. Subsequently, we derived the parameters associated with charge recombination from Figure 2d by using use eqs 4 and 5[38,39]

$$n(t) = \frac{n(0)}{1 + \left(\frac{t}{\tau_B}\right)^{\gamma}} \tag{4}$$

$$\beta_L = \frac{e \times \mu}{\varepsilon \times \varepsilon_0} \tag{5}$$

where τ_B is the effective second-order recombination coefficient, γ is the time-independent parameter, and β_L is the Langevin recombination coefficient. All of these results are summarized in Table 1. Note that when γ is close to 1, a nondispersive bimolecular recombination takes place. Bimolecular recombination occurs between free charge carriers, while trap-assisted recombination in previous discussion relates to monomolecular recombination. Our result shows that γ is 0.686, meaning that bimolecular recombination in perovskite solar cells is comparatively dispersive owing to the presence of shallow traps, which is consistent with the TOF results.

Apart from their light instability, perovskite solar cells are very sensitive to device temperature.[11−14] Therefore, we performed temperature-dependent TOF and electrical conductivity measurements to investigate the origin of thermal instability in perovskite solar cells. The TOF $j-t$ profiles as a function of temperature are displayed in Figure S3, and the temperature dependences of hole and electron mobilities are presented in Figure 3.

In hole measurements (Figure S3a,b), the t_{tr} first increases slightly when the temperature is increased from 295 to 310 K and then decreases rapidly when it is further increased to 330 K. As a result, the highest hole mobility reaches 1.95×10^{-4} $cm^2/(V\ s)$ at 310 K, while the lowest is 5.92×10^{-5} $cm^2/(V\ s)$ at 325 K, as seen from Figure 3. By comparison, the

DOI: 10.1021/acsenergylett.6b00393
ACS Energy Lett. 2016, 1, 1000−1006

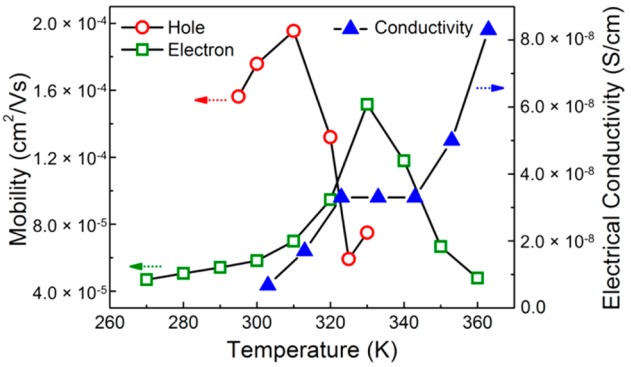

Figure 3. Temperature dependences of both charge mobilities of $CH_3NH_3PbI_3$/PCBM bilayer cells and dark conductivities of $CH_3NH_3PbI_3$ neat films.

temperature dependence of the electron mobility is slightly different from that of hole mobility. In electron measurements (Figure S3c–e), the t_{tr} increases when the temperature is increased from 270 to 330 K, followed by a rapid decrease of t_{tr} when it is further increased from 330 to 360 K. The highest electron mobility of 1.52×10^{-4} $cm^2/(V\ s)$ is obtained at 330 K, as seen from Figure 3.

As shown in Figure 3, the maximum and minimum of carrier mobilities can be obtained in the temperature range between 310 and 330 K. At 320 K, both hole (1.32×10^{-4} $cm^2/(V\ s)$) and electron (9.46×10^{-5} $cm^2/(V\ s)$) mobilities become most balanced. Interestingly, the phase transition of perovskites has also been reported to occur in the same temperature range.[40] For instance, Milot et al. observed a phase transition of perovskites from tetragonal to cubic at 310 K,[12] and Weller et al. reported that the tetragonal phase of perovskites is only stable between 165 and 327 K,[13] both of which coincide with our temperature results.

Meanwhile, electrical conductivity measurement in the dark was used to substantiate the above temperature influences on charge transport. As shown in Figure 3, when the temperature is increased from 303 to 323 K and 343 to 363 K, the conductivity of the neat $CH_3NH_3PbI_3$ film is gradually increased. This positive temperature tendency of perovskite conductivity is consistent with the literature report.[41] However, the conductivity value is maintained when the temperature changes from 323 to 343 K, which is exactly located within the temperature range of the phase transition. This strongly indicates that electrical conductivity tends to remain unchanged during the phase transition, regardless of varied temperatures.

To further unveil the above transport behavior, $\log(\mu)$ versus $\log(T)$ curves based on the TOF electron data are first linearly fitted by the equation $\mu \propto T^n$ (Figure S4a),[42] yielding n = 5.3 over 270–330 K and −13.9 over 330–360 K, respectively. The positive and negative n values obtained within different temperature ranges suggest that the hopping conduction dominates in the tetragonal phase while the band-like conduction plays a key role in the cubic phase of perovskites. Then, the Arrhenius fit is applied to extract the activation energy (E_a) of electron mobility results by the equation $\mu \propto e^{-E_a/(kT)}$, where k is the Boltzmann constant (Figure S4b).[43] As a result, E_a is calculated as 51.7 meV over 270–360 K, which is comparatively lower than the previously reported E_a of 74.4 meV in the two-step fabricated $CH_3NH_3PbI_3$-based inverted solar cells.[44] This phenomenon implies that the shallower trap states exist in regular perovskite solar cells than inverted analogues, which is also consistent with the observation of a shallow trap filling process in TOF measurements.

Lastly, the influences of light and heat on charge transport are schematically summarized in Figure 4a,b, respectively.

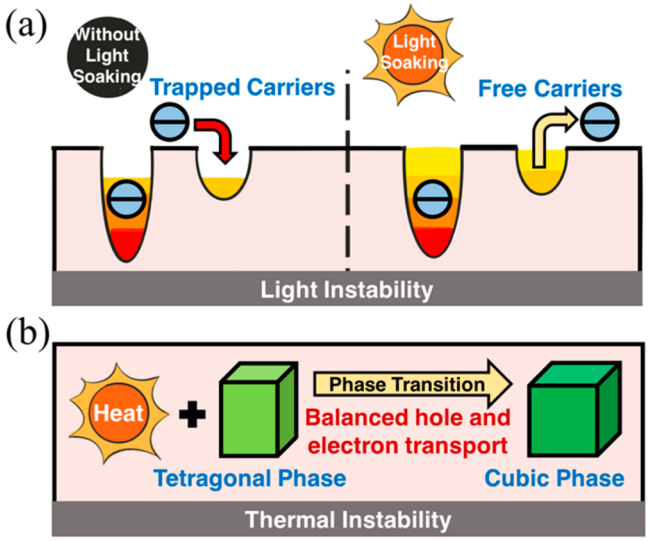

Figure 4. Illustrative charge transport process in perovskite solar cells influenced by (a) light soaking and (b) phase transition.

Figure 4a shows the existence of shallow traps caused by morphological defects at the interface between $CH_3NH_3PbI_3$ and PCBM. Upon continuous light illumination, a process of shallow trap filling reversibly occurs until a stable equilibrium, resulting in significantly increased hole and electron mobilities. As a result, when measuring light J–V curves, an increased V_{OC} yet maintained J_{SC} is observed, implying that the light soaking process assists in reducing trap-assisted charge recombination and then improves the device performance. As shown in Figure 4b, when the temperature is increased from 310 to 330 K, corresponding to a phase transition of perovskites from tetragonal to cubic structures,[11] a decrease of the hole mobility while an increase of the electron mobility is found until there is a balance of charge transport, which yields the best cell performance. In addition, the hole mobility of the tetragonal phase is found to be remarkably higher than that of the cubic phase, indicative of different transport dynamics at various perovskite phases.

To conclude, we have systematically studied the influences of light soaking and thermal phase transition on charge transport dynamics in two-step fabricated $CH_3NH_3PbI_3$ perovskite solar cells by combining TOF, CELIV, and electrical conductivity measurements. The nondispersive charge transport is unveiled in perovskite solar cells, which is distinctive from dispersive transport of most organic semiconductors and their solar cells. Meanwhile, we directly observe a reversible shallow trap filling process during light soaking, which leads to remarkably increased carrier mobilities. This indicates that light soaking plays a critical role in suppressing trap-assisted charge recombination and improving cell performance. Moreover, we surprisingly find a rapid change of both hole and electron mobilities during phase transition from tetragonal to cubic crystalline structures at around 310–330 K until reaching a balance of hole and electron transport, which gives rise to the best cell performance.

DOI: 10.1021/acsenergylett.6b00393
ACS Energy Lett. 2016, 1, 1000–1006

■ ASSOCIATED CONTENT

Supporting Information

The Supporting Information is available free of charge on the ACS Publications website at DOI: 10.1021/acsenergylett.6b00393.

Details of all experimental procedures, representative *J*–*V* curves and TOF *j*–*t* double-logarithmic profiles of hole and electron measurements as a function of temperature in $CH_3NH_3PbI_3$/PCBM bilayer solar cells, and FE-SEM images of the $CH_3NH_3PbI_3$ neat film and $CH_3NH_3PbI_3$/PCBM bilayer film (PDF)

■ AUTHOR INFORMATION

Corresponding Authors

*E-mail: yaoyao@fudan.edu.cn (Y.Y.).
*E-mail: zqliang@fudan.edu.cn (Z.L.).

Notes

The authors declare no competing financial interest.

■ ACKNOWLEDGMENTS

This work was supported by National Natural Science Foundation of China (NSFC) under Grant 51473036 (Z.L.). Y.Y. gratefully acknowledges financial support from NSFC under Grants 91333202 and 11574052 and the National Basic Research Program of China under Grant 2012CB921401.

■ REFERENCES

(1) Chen, Y.; He, M.; Peng, J.; Sun, Y.; Liang, Z. Structure and Growth Control of Organic–Inorganic Halide Perovskites for Optoelectronics: From Polycrystalline Films to Single Crystals. *Adv. Sci.* **2016**, *3*, 1500392.

(2) Hu, M.; Bi, C.; Yuan, Y.; Xiao, Z.; Dong, Q.; Shao, Y.; Huang, J. Distinct Exciton Dissociation Behavior of Organolead Trihalide Perovskite and Excitonic Semiconductors Studied in the Same System. *Small* **2015**, *11*, 2164–2169.

(3) Stranks, S. D.; Eperon, G. E.; Grancini, G.; Menelaou, C.; Alcocer, M. J. P.; Leijtens, T.; Herz, L. M.; Petrozza, A.; Snaith, H. J. Electron-Hole Diffusion Lengths Exceeding 1 Micrometer in an Organometal Trihalide Perovskite Absorber. *Science* **2013**, *342*, 341–344.

(4) Oga, H.; Saeki, A.; Ogomi, Y.; Hayase, S.; Seki, S. Improved Understanding of the Electronic and Energetic Landscapes of Perovskite Solar Cells: High Local Charge Carrier Mobility, Reduced Recombination, and Extremely Shallow Traps. *J. Am. Chem. Soc.* **2014**, *136*, 13818–13825.

(5) Bi, D.; Tress, W.; Dar, M. I.; Gao, P.; Luo, J.; Renevier, C.; Schenk, K.; Abate, A.; Giordano, F.; Correa Baena, J.-P.; et al. A. Efficient Luminescent Solar Cells Based on Tailored Mixed-Cation Perovskites. *Sci. Adv.* **2016**, *2*, e1501170.

(6) Kojima, A.; Teshima, K.; Shirai, Y.; Miyasaka, T. Organometal Halide Perovskites as Visible-Light Sensitizers for Photovoltaic Cells. *J. Am. Chem. Soc.* **2009**, *131*, 6050–6051.

(7) Conings, B.; Drijkoningen, J.; Gauquelin, N.; Babayigit, A.; D'Haen, J.; D'Olieslaeger, L.; Ethirajan, A.; Verbeeck, J.; Manca, J.; Mosconi, E.; et al. Intrinsic Thermal Instability of Methylammonium Lead Trihalide Perovskite. *Adv. Energy Mater.* **2015**, *5*, 1500477.

(8) Leijtens, T.; Eperon, G. E.; Pathak, S.; Abate, A.; Lee, M. M.; Snaith, H. J. Overcoming Ultraviolet Light Instability of Sensitized TiO_2 with Meso-Superstructured Organometal Tri-Halide Perovskite Solar Cells. *Nat. Commun.* **2013**, *4*, 2885.

(9) Deng, Y.; Xiao, Z.; Huang, J. Light-Induced Self-Poling Effect on Organometal Trihalide Perovskite Solar Cells for Increased Device Efficiency and Stability. *Adv. Energy Mater.* **2015**, *5*, 1500721.

(10) Zhao, C.; Chen, B.; Qiao, X.; Luan, L.; Lu, K.; Hu, B. Revealing Underlying Processes Involved in Light Soaking Effects and Hysteresis Phenomena in Perovskite Solar Cells. *Adv. Energy Mater.* **2015**, *5*, 1500279.

(11) Leong, W. L.; Ooi, Z.-E.; Sabba, D.; Yi, C.; Zakeeruddin, S. M.; Graetzel, M.; Gordon, J. M.; Katz, E. A.; Mathews, N. Identifying Fundamental Limitations in Halide Perovskite Solar Cells. *Adv. Mater.* **2016**, *28*, 2439–2445.

(12) Milot, R. L.; Eperon, G. E.; Snaith, H. J.; Johnston, M. B.; Herz, L. M. Temperature-Dependent Charge-Carrier Dynamics in $CH_3NH_3PbI_3$ Perovskite Thin Films. *Adv. Funct. Mater.* **2015**, *25*, 6218–6217.

(13) Weller, M. T.; Weber, O. J.; Henry, P. F.; Di Pumpo, A. M.; Hansen, T. C. Complete Structure and Cation Orientation in the Perovskite Photovoltaic Methylammonium Lead Iodide between 100 and 352 K. *Chem. Commun.* **2015**, *51*, 4180–4183.

(14) Quarti, C.; Mosconi, E.; Ball, J. M.; D'Innocenzo, V.; Tao, C.; Pathak, S.; Snaith, H. J.; Petrozza, A.; De Angelis, F. Structural and Optical Properties of Methylammonium Lead Iodide across the Tetragonal to Cubic Phase Transition: Implications for Perovskite Solar Cells. *Energy Environ. Sci.* **2016**, *9*, 155–163.

(15) Mosconi, E.; Meggiolaro, D.; Snaith, H. J.; Stranks, S. D.; De Angelis, F. Light-Induced Annihilation of Frenkel Defects in Organo-Lead Halide Perovskites. *Energy Environ. Sci.* **2016**, *9*, 3180–3187.

(16) Chen, Y.; Peng, J.; Su, D.; Chen, X.; Liang, Z. Efficient and Balanced Charge Transport Revealed in Planar Perovskite Solar Cells. *ACS Appl. Mater. Interfaces* **2015**, *7*, 4471–4475.

(17) Peng, J.; Chen, X.; Chen, Y.; Sandberg, O. J.; Österbacka, R.; Liang, Z. Transient Extraction of Holes and Electrons Separately Unveils the Transport Dynamics in Organic Photovoltaics. *Adv. Electron. Mater.* **2016**, *2*, 1500333.

(18) Pivrikas, A.; Sariciftci, N. S.; Juška, G.; Österbacka, R. A Review of Charge Transport and Recombination in Polymer/Fullerene Organic Solar Cells. *Prog. Photovoltaics* **2007**, *15*, 677–696.

(19) Burschka, J.; Pellet, N.; Moon, S.-J.; Humphry-Baker, R.; Gao, P.; Nazeeruddin, M. K.; Grätzel, M. Sequential Deposition as A Route to High-Performance Perovskite-Sensitized Solar Cells. *Nature* **2013**, *499*, 316–320.

(20) Collavini, S.; Völker, S. F.; Delgado, J. L. Understanding the Outstanding Power Conversion Efficiency of Perovskite-Based Solar Cells. *Angew. Chem., Int. Ed.* **2015**, *54*, 9757–9759.

(21) Lin, Q.; Armin, A.; Burn, P. L.; Meredith, P. Organohalide Perovskites for Solar Energy Conversion. *Acc. Chem. Res.* **2016**, *49*, 545–553.

(22) Tuladhar, S. M.; Poplavskyy, D.; Choulis, S. A.; Durrant, J. R.; Bradley, D. D.; Nelson, J. Ambipolar Charge Transport in Films of Methanofullerene and Poly (phenylenevinylene)/Methanofullerene Blends. *Adv. Funct. Mater.* **2005**, *15*, 1171–1182.

(23) de Haas, M. P.; Warman, J. M.; Anthopoulos, T. D.; de Leeuw, D. M. The Mobility and Decay Kinetics of Charge Carriers in Pulse-Ionized Microcrystalline PCBM Powder. *Adv. Funct. Mater.* **2006**, *16*, 2274–2280.

(24) Steirer, K. X.; Schulz, P.; Teeter, G.; Stevanovic, V.; Yang, M.; Zhu, K.; Berry, J. J. Defect Tolerance in Methylammonium Lead Triiodide Perovskite. *ACS Energy Lett.* **2016**, *1*, 360–366.

(25) Herz, L. M. Charge-Carrier Dynamics in Organic-Inorganic Metal Halide Perovskites. *Annu. Rev. Phys. Chem.* **2016**, *67*, 65–89.

(26) Li, C.; Duan, L.; Li, H.; Qiu, Y. Universal Trap Effect in Carrier Transport of Disordered Organic Semiconductors: Transition from Shallow Trapping to Deep Trapping. *J. Phys. Chem. C* **2014**, *118*, 10651–10660.

(27) Giebink, N. C.; Wiederrecht, G. P.; Wasielewski, M. R.; Forrest, S. R. Ideal Diode Equation for Organic Heterojunctions. I. Derivation and Application. *Phys. Rev. B: Condens. Matter Mater. Phys.* **2010**, *82*, 155305.

(28) Sandberg, O. J.; Sundqvist, A.; Nyman, M.; Österbacka, R. Relating Charge Transport, Contact Properties, and Recombination to Open-Circuit Voltage in Sandwich-Type Thin-Film Solar Cells. *Phys. Rev. Appl.* **2016**, *5*, 044005.

(29) Ahn, N.; Son, D.-Y.; Jang, I.-H.; Kang, S. M.; Choi, M.; Park, N.-G. Highly Reproducible Perovskite Solar Cells with Average Efficiency

DOI: 10.1021/acsenergylett.6b00393
ACS Energy Lett. 2016, 1, 1000–1006

of 18.3% and Best Efficiency of 19.7% Fabricated via Lewis Base Adduct of Lead(II) Iodide. *J. Am. Chem. Soc.* **2015**, *137*, 8696−8699.
(30) Xing, G.; Mathews, N.; Sun, S.; Lim, S. S.; Lam, Y. M.; Grätzel, M.; Mhaisalkar, S.; Sum, T. C. Long-Range Balanced Electron and Hole-Transport Lengths in Organic-Inorganic $CH_3NH_3PbI_3$. *Science* **2013**, *342*, 344−347.
(31) Kim, H.-S.; Lee, C.-R.; Im, J.-H.; Lee, K.-B.; Moehl, T.; Marchioro, A.; Moon, S.-J.; Humphry-Baker, R.; Yum, J.-H.; Moser, J. E.; et al. Lead Iodide Perovskite Sensitized All-Solid-State Submicron Thin Film Mesoscopic Solar Cell with Efficiency Exceeding 9%. *Sci. Rep.* **2012**, *2*, 591.
(32) Dualeh, A.; Moehl, T.; Tétreault, N.; Teuscher, J.; Gao, P.; Nazeeruddin, M. K.; Grätzel, M. Impedance Spectroscopic Analysis of Lead-Iodide Perovskite-Sensitized Solid-State Solar Cells. *ACS Nano* **2014**, *8*, 362−373.
(33) Oga, H.; Saeki, A.; Ogomi, Y.; Hayase, S.; Seki, S. Improved Understanding of the Electronic and Energetic Landscapes of Perovskite Solar Cells: High Local Charge Carrier Mobility, Reduced Recombination, and Extremely Shallow Traps. *J. Am. Chem. Soc.* **2014**, *136*, 13818−13825.
(34) Marchioro, A.; Teuscher, J.; Friedrich, D.; Kunst, M.; van de Krol, R.; Moehl, T.; Grätzel, M.; Moser, J.-E. Unravelling the Mechanism of Photoinduced Charge Transfer Processes in Lead Iodide Perovskite Solar Cells. *Nat. Photonics* **2014**, *8*, 250−255.
(35) Ponseca, C. S., J.; Savenije, T. J.; Abdellah, M.; Zheng, K.; Yartsev, A.; Pascher, T. r.; Harlang, T.; Chabera, P.; Pullerits, T.; Stepanov, A.; et al. Organometal Halide Perovskite Solar Cell Materials Rationalized: Ultrafast Charge Generation, High and Microsecond-Long Balanced Mobilities, and Slow Recombination. *J. Am. Chem. Soc.* **2014**, *136*, 5189−5192.
(36) Dong, Q.; Fang, Y.; Shao, Y.; Mulligan, P.; Qiu, J.; Cao, L.; Huang, J. Electron-Hole Diffusion Lengths > 175 μm in Solution-Grown $CH_3NH_3PbI_3$ Single Crystals. *Science* **2015**, *347*, 967−970.
(37) Amonoo, J. A.; Li, A.; Purdum, G. E.; Sykes, M. E.; Huang, B.; Palermo, E. F.; McNeil, A. J.; Shtein, M.; Loo, Y.-L.; Green, P. F. An All-Conjugated Gradient Copolymer Approach for Morphological Control of Polymer Solar Cells. *J. Mater. Chem. A* **2015**, *3*, 20174−20184.
(38) Mohammad, L.; Chen, Q.; Mitul, A.; Sun, J.; Khatiwada, D.; Vaagensmith, B.; Zhang, C.; Li, J.; Qiao, Q. Improved Performance for Inverted Organic Photovoltaics via Spacer between Benzodithiophene and Benzothiazole in Polymers. *J. Phys. Chem. C* **2015**, *119*, 18992−19000.
(39) Min, J.; Luponosov, Y. N.; Gasparini, N.; Richter, M.; Bakirov, A. V.; Shcherbina, M. A.; Chvalun, S. N.; Grodd, L.; Grigorian, S.; Ameri, T.; et al. Effects of Alkyl Terminal Chains on Morphology, Charge Generation, Transport, and Recombination Mechanisms in Solution-Processed Small Molecule Bulk Heterojunction Solar Cells. *Adv. Energy Mater.* **2015**, *5*, 1500386.
(40) Hoque, M. N. F.; Yang, M.; Li, Z.; Islam, N.; Pan, X.; Zhu, K.; Fan, Z. Polarization and Dielectric Study of Methylammonium Lead Iodide Thin Film to Reveal its Nonferroelectric Nature under Solar Cell Operating Conditions. *ACS Energy Lett.* **2016**, *1*, 142−149.
(41) Sveinbjörnsson, K. i.; Aitola, K.; Zhang, X.; Pazoki, M.; Hagfeldt, A.; Boschloo, G.; Johansson, E. M. J. Probing Photocurrent Generation, Charge Transport, and Recombination Mechanisms in Mesostructured Hybrid Perovskite through Photoconductivity Measurements. *J. Phys. Chem. Lett.* **2015**, *6*, 4259−4264.
(42) Coropceanu, V.; Cornil, J.; da Silva Filho, D. A.; Olivier, Y.; Silbey, R.; Brédas, J.-L. Charge Transport in Organic Semiconductors. *Chem. Rev.* **2007**, *107*, 926−952.
(43) Craciun, N. I.; Wildeman, J.; Blom, P. W. M. Universal Arrhenius Temperature Activated Charge Transport in Diodes from Disordered Organic Semiconductors. *Phys. Rev. Lett.* **2008**, *100*, 056601.
(44) Chen, Q.; Zhou, H.; Fang, Y.; Stieg, A. Z.; Song, T.-B.; Wang, H.-H.; Xu, X.; Liu, Y.; Lu, S.; You, J.; et al. The Optoelectronic Role of Chlorine in $CH_3NH_3PbI_3$(Cl)-Based Perovskite Solar Cells. *Nat. Commun.* **2015**, *6*, 7269.

DOI: 10.1021/acsenergylett.6b00393
ACS Energy Lett. 2016, 1, 1000−1006